



# Photo-catalytic dye degradation of methyl orange using zirconia–zeolite nanoparticles

M MANSOURI<sup>1,\*</sup>, N MOZAFARI<sup>1</sup>, B BAYATI<sup>1</sup> and N SETARESHENAS<sup>2</sup>

<sup>1</sup>Department of Chemical Engineering, Ilam University, Ilam 69315-516, Iran

<sup>2</sup>Department of Chemical Engineering, Eyvan-e-Gharb Branch, Islamic Azad University, Eyvan 694111-1359, Iran

\*Author for correspondence (mansouri2010@yahoo.com; m.mansouri@ilam.ac.ir)

MS received 24 February 2019; accepted 17 May 2019; published online 12 July 2019

**Abstract.** In this research, the dye photo-catalytic removal was investigated using zirconia (ZrO<sub>2</sub>) nanocatalysts, zeolite (Ze), ZrO<sub>2</sub>–Ze with different percentages and optimized ZrO<sub>2</sub>–Ze doped *via* urea, copper oxide and cerium oxide. In order to determine the optimal conditions, the effects of different catalysts and parameters such as dye concentration, UV lamp power, amount of the loaded catalyst and pH were investigated. The response surface methodology was used to obtain optimal experimental conditions. Physical and chemical properties of materials were investigated by X-ray diffraction, Fourier transform infrared, scanning electron microscopy and Brunauer–Emmett–Teller. Completely methyl orange (MO)-dye removal (100%) was achieved at optimal conditions under UV light during 80 min. The optimal operational condition for MO photo-catalytic decomposition using an optimal N-doped 10 wt% ZrO<sub>2</sub>–zeolite nanocatalyst was obtained at UV lamp power, pH, catalyst loading and dye concentration of 15 W, 3, 0.4 g l<sup>-1</sup> and 5 mg l<sup>-1</sup>, respectively. Photo-catalytic degradation kinetics of MO described well using pseudo-first order which is in accordance with the Langmuir–Hinshelwood model ( $k_{app} = 0.031 \text{ min}^{-1}$ ).

**Keywords.** Advanced oxidation; N-doped zirconia–zeolite; experimental design; optimization; nanocatalyst.

## 1. Introduction

The photo-catalytic process has been successfully used to remove a wide range of pollutants such as dyes, phenols, surfactants, aromatic hydrocarbons and pesticides. The process is based on the production of highly active species (i.e., hydroxyl radicals) that have high oxidizing ability with dye molecules. This act causes decomposition of dyes and removal from water and wastewaters [1]. Due to high optical, electrical and catalytic properties, titania and zirconia nano-photocatalysts have a great potential to be considered as catalysts for water and wastewater treatment [1,2]. Recently, zirconia has been attracted more attention among the photocatalysts due to its biological and chemical ineffectiveness, lack of toxicity, good environmental stability at aqueous solution and safe applications [2]. In the literature reported that ZrO<sub>2</sub> structural changing, porosity controlling and crystallization developing are effective factors to increase the removal capacity of pollutants [3].

Low adsorption and surface area are the most important limitations for photocatalyst efficiency. Therefore, the stabilization of semiconductors on suitable supports can overcome these limitations with an increase in the separation of charges, an increase in the lifespan of the charge carriers, an increase in charge surface transfer to adsorbent substrates and the reduction of cost. Zeolites are suitable supports for this work due to its three-dimensional crystalline structure, high-physical

and chemical resistance, uniform holes and channels, high surface areas, excellent adsorption capacity and unique structures. Among the zeolites, synthesized zeolites have more advantages than natural zeolites because they are synthesized with a pure phase and uniformity. In addition, the synthesized zeolites can be produced with a wide range of pore sizes [4–6]. The removal of various compounds including Reactive Black-5 [4], Brown-NG [5] and methyl orange (MO) [6] by titanium dioxide stabilized on the surface of zeolites has been performed in several studies. The results of these studies show the efficiency and degradation rate (about 98%) of this photocatalyst compared with the use of pure titanium dioxide as a catalyst. In the study presented by Bhattacharjee *et al*, the photo-catalytic degradation of Reactive Black-5 dye was investigated using a TiO<sub>2</sub> photocatalyst under UV radiation from aqueous solution. They investigated the effect of UV irradiation and pH of solution on the dye removal, and reported the dye removal of 94 and 75% at pH of 6.4 and 4.8, respectively [7]. The results of Panpa *et al* on methylene blue photocatalytic degradation using a TiO<sub>2</sub>@ZSM5 photocatalyst showed that the dye removal using this photocatalyst at 2.5 h was higher than that for pure TiO<sub>2</sub> which leads to complete dye removal [8].

Zhao *et al* synthesized ZnO nanotubes using a coating method and obtained the nanotubes with a length distribution of 25 μm, an internal diameter of 80 nm and a thickness of 35 nm. They observed that 97.6% of the MO dye (soluble

in water) could remove over a period of 8 h at a pH of 13 [9]. Ismail *et al* synthesized nanotubes of zirconia and tested their photo-catalytic ability. They found 30% of MO removal in the presence of ZrO<sub>2</sub> nanotubes after 120 min under ultraviolet light [10].

Basahel *et al* investigated the effect of the crystalline structure of ZrO<sub>2</sub> nanoparticles on the photocatalytic decomposition of MO. They synthesized triangular, tetrahedral and monoclinic phases of ZrO<sub>2</sub> porous nanoparticles with different methods and measured the photocatalytic performance of three-ZrO<sub>2</sub> samples for the decomposition of MO. They showed that, under optimal operating conditions, the m-ZrO<sub>2</sub> sample (monoclinic) had more decomposition for MO compared to t-ZrO<sub>2</sub> (tetrahedral) and c-ZrO<sub>2</sub> (cubic) samples. The catalytic activity specified for the m-ZrO<sub>2</sub> sample catalyst was strongly influenced by the effects of factors such as the presence of a small amount of the zirconium dioxide phase, crystallinity, pore size distribution and high density of hydroxyl groups in the surface [11].

The effect of the doping of semiconductors has also been studied in the research. Yoa *et al* examined the photocatalytic decomposition of the MO dye using lanthanum (nanomagnets)-doped-titanium dioxide nanocatalysts. The nanoparticles were synthesized by the sol-gel method, and dye decomposition was reported as 85% in an optimum molar percentage of 0.15 [12]. Mzoughi *et al* studied the photocatalytic activity of removing Eosin Y dye in aqueous solution under sunlight by synthesized zirconium dioxide and Nd-ZrO<sub>2</sub>-G. It was observed that the Nd-ZrO<sub>2</sub>-G catalyst has the potential to degrade the dye compared to the zirconium dioxide. Using a 0.3 wt% Nd-ZrO<sub>2</sub>-G catalyst, 80% dye removal was performed in 180 min [13].

As earlier studies have shown, the stabilized zirconium dioxide on the zeolite surfaces has not yet been studied in the research. Therefore, the aim of the present study is to synthesize a photocatalyst with zeolite content and coated with ZrO<sub>2</sub> nanoparticles, which are doped by metals such as cerium oxide, copper oxide and non-metallic such as urea. Further, the physical and chemical properties of the photo-catalyst were investigated by various characterization techniques. Also, the photo-catalytic properties of the product were tested to remove MO dye under UV light. In order to determine the optimal conditions for high-performance dye removal, the effect of operational parameters on the photocatalytic degradation, including pH, dye concentration, lamp power and amount of loaded photocatalyst was investigated under UV light.

## 2. Methods

### 2.1 Materials

Zirconium(IV) propoxide (Zr[O(CH<sub>2</sub>)<sub>2</sub>CH<sub>3</sub>]<sub>4</sub>), copper nitrate (Cu(NO<sub>3</sub>)<sub>2</sub>·6H<sub>2</sub>O), cerium nitrate (Ce(NO<sub>3</sub>)<sub>3</sub>·6H<sub>2</sub>O), urea (NH<sub>2</sub>CONH<sub>2</sub>) materials, sodium hydroxide (NaOH), sodium

aluminate (AlNaO<sub>2</sub>), acetic acid (CH<sub>3</sub>COOH), isopropanol (C<sub>3</sub>H<sub>7</sub>OH) and nitric acid (HNO<sub>3</sub>) were all of analytical grade, purchased from Aldrich, USA, and used without further purification. Also, tetraethyl orthosilicate (TEOS, C<sub>8</sub>H<sub>20</sub>O<sub>4</sub>Si) and MO (C<sub>14</sub>H<sub>14</sub>N<sub>3</sub>NaO<sub>3</sub>S) were purchased from Merck, Germany.

### 2.2 Instruments

The X-ray diffraction (XRD) patterns of the prepared materials were recorded on an X-ray diffractometer (Siemens D5000) using Ni filtered CuK $\alpha$  radiation from  $2\theta = 2-80^\circ$ . The crystalline size of nanoparticles is computed using obtained information from XRD and the Scherrer equation. A scanning electron microscope (SEM, Leo 1455 VP) was used for the identification of nanoparticle surface morphological features. A UV-Vis spectrophotometer (Model T80+, PG Instruments, UK) was used for measuring the amount of residual MO. A TRB-5 quartz capillary column of 30 m  $\times$  0.53 mm with a 3  $\mu$ m film thickness was used in a UV-Vis spectrophotometer. To analyse the chemical structure of samples, Fourier transform infrared (FTIR) spectroscopy absorption spectra for all samples were recorded in the range of 400–4000 cm<sup>-1</sup> with a 460 Plus Jasco spectrophotometer (USA) using KBr pellets at room temperature. Each sample was recorded with 32 scans at an effective resolution of 4 cm<sup>-1</sup>. The specific surface area of each sample was calculated by using the Brunauer-Emmett-Teller (BET) method (UPA-150, Microtrac).

### 2.3 Nanoparticle synthesis

In this research, the ZrO<sub>2</sub> nanocatalysts, zeolite and ZrO<sub>2</sub>-Ze nanocatalysts with different percentages and optimized ZrO<sub>2</sub>-Ze doped *via* urea, copper oxide and cerium oxide were used for MO photocatalytic removal. The methods for their synthesis are as follows.

### 2.4 Synthesis of zeolite-NaX

The used zeolite in this study is NaX type which is synthesized as follows. Firstly, 49.14 ml of distilled water was added into a 100 ml beaker, then 4.37 g of sodium hydroxide and 3.06 g of sodium aluminate were added to the solution. The solution was agitated until well dissolved. In this case, the temperature of the solution is raised, hence it is placed in a cold water bath until temperature reaches to an ambient level. Then, 7.93 ml of TEOS was poured into the burette, added dropwise to the solution and stirred for 40 min. The solution was transferred to an autoclave and placed in an oven at 90°C for 15 h. After this period, the solution was filtered and the attained precipitate was mixed with a large amount of distilled water and agitated for 1 h. This solution was aged for one day to precipitate. The precipitate was washed until to achieve natural pH and finally dried in an oven at 100°C for 24 h.

## 2.5 Zirconia nanoparticle synthesis

The ZrO<sub>2</sub> nanoparticles were synthesized by the sol–gel method. Firstly, the solution containing zirconium(IV) propoxide is added to isopropanol with a molar ratio of 1 Zr : 15 isopropanol. After the solution becomes completely uniform, dilute nitric acid is added slowly to it using the burette. The total solution was kept at 30°C and stirred by the magnet for 50 min (when the total nitric acid was added to the solution). The added nitric acid reacted with an alcohol which causes the decomposition of H<sub>2</sub>O and creates the catalytic properties. The molar ratio of solution compounds was 1.0 H<sub>2</sub>O : 0.6 HNO<sub>3</sub> : 7.5 isopropanol. After the solution being completely uniform, it was agitated for 2 h until the gel was prepared. The pH was increased from 2 to 3 over the duration of the gel creation. The resulting mixture was then dried at 120°C for 12 h. After drying, the catalyst precursor was calcined using an electrical furnace at 600°C under an air atmosphere for 6 h.

## 2.6 Synthesis of doped zirconia–zeolite nanoparticles

The zirconia with various weight ratios of 10, 30, 50 and 70% was used to achieve the optimum value for the zirconia–zeolite catalyst. After zeolite synthesis, it was weighed to the required amount and added to the solution containing zirconium(IV) propoxide and isopropanol with a specified ratio. The continuation of the synthesis process is similar to the synthesis of zirconia nanocatalysts. The synthesis of the zirconia–zeolite catalyst doped by 0.3 mol of various promoters (urea, copper oxide and cerium oxide) is similar to the above mentioned procedure.

## 2.7 MO photocatalytic decomposition procedure

The photo-catalytic decomposition of MO was carried out by a cylindrical Pyrex reactor with a length of 460 mm and a volume of 1 l. The reactor has a valve for sampling during the process, and the contents are exposed to a UVC-lamp with varying powers of 4, 8 and 15 W. The solution in the reactor circulates in a closed cycle between the tank of a pump and the reactor inside. The SOBO aquarium pump with a power of 15 W and a flow rate of 2 l min<sup>-1</sup> was used to flow inside the reactor. The investigated parameters in the process include the UV lamp power, the amount of catalyst (catalyst dosage), dye concentration and pH. To determine the adsorbance of the synthesized catalysts, the solution was poured into the reactor, and the pump was switched on for 30 min in the dark mode to bring about adsorption on the surface of the nanocatalysts. The solution was then exposed to UV light for 80 min; the amount removed was measured using a UV instrument at different times (at a wavelength of 508 nm). The percentage of dye removal was also calculated by using the following equation:

$$X = \frac{C_0 - C}{C_0} \times 100, \quad (1)$$

where  $C_0$  and  $C$  are the initial and final concentrations, respectively. To avoid any error, tests were repeated at three times. The standard error (SE) of the data is also calculated by dividing standard deviation (SD) by the number of repeated experiments in accordance with the following

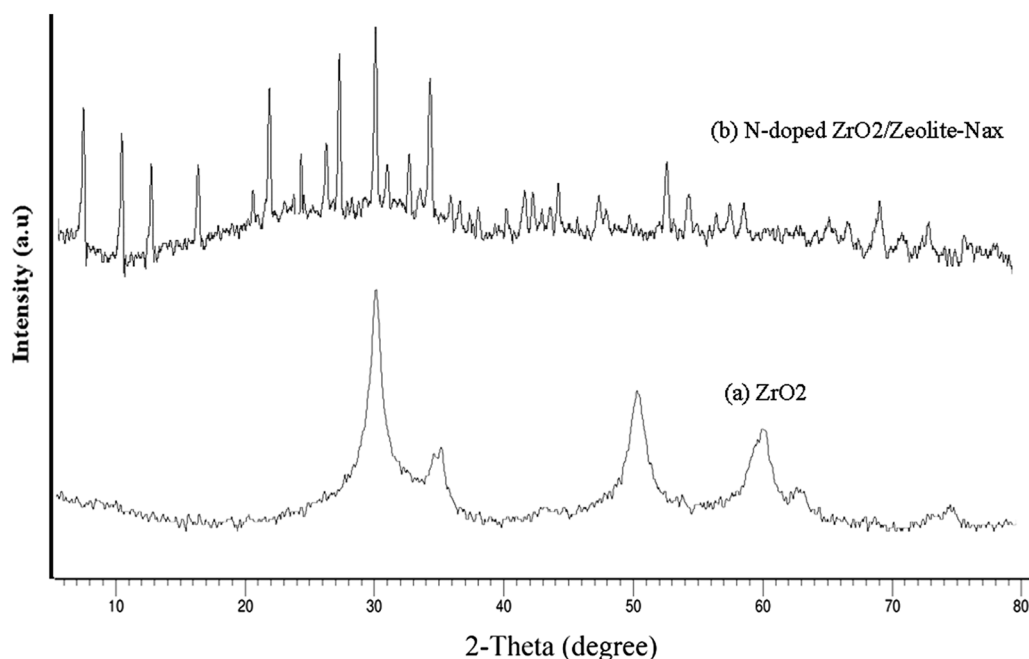


**Figure 1.** XRD patterns of (a) ZrO<sub>2</sub> and (b) N-doped ZrO<sub>2</sub>–zeolite–NaX.

equation:

$$SE = \frac{SD}{\sqrt{N}}, \quad (2)$$

$$SD = \sqrt{\frac{\sum (X - \bar{X})^2}{N - 1}}, \quad (3)$$

where  $N$  is the number of repetitions.  $X$  and  $\bar{X}$  are the percentage of colour removal at each test and at the mean of repetitions, respectively.

### 3. Results and discussion

#### 3.1 Characterization of nanoparticles

XRD was used to determine the crystalline structure of synthesized zeolite–NaX,  $ZrO_2$  nanoparticles and N-doped  $ZrO_2$ –Ze, and results are shown in figure 1. The X-ray  $2\theta$  diffraction lines show the existence of two nanocrystals for zirconia (figure 1a), the monoclinic phase at  $2\theta = 30.47, 36.78, 50.17$  and  $63.81$  according to JCPDS 37-1484 and the tetragonal phase at  $2\theta = 35.19, 47.67, 59.16$  and  $74.69$  according to JCPDS 80-0965. Also, the peaks/lines that indicate impurities in the material are not seen in this pattern. The obtained XRD pattern for N-doped  $ZrO_2$ –Ze is shown in figure 1b. The sharp peaks in the  $2\theta$  ranges of  $3$ – $35^\circ$  indicate that the structure of zeolite is well crystallized. The NaX phase was identified on the basis of a group of characteristics of their reflections ( $d_{hkl} = 7.54, 10.55, 12.94, 16.47, 27.42$  and  $52.73$ ). The detailed JCPDS pattern lines for zeolite–NaX are already mentioned in the literature [7]. The zirconia peaks are distinctly seen in both  $ZrO_2$  and N-doped  $ZrO_2$ –Ze–NaX. The XRD pattern given in figure confirms the presence of urea through peaks at  $2\theta = 22.20, 47.16$  and  $73.13^\circ$ . This shows the formation of urea and  $ZrO_2$  nanoparticles over the formed zeolite framework. The average crystallite sizes of the photocatalysts are:  $ZrO_2 = 7.13$  nm and N-doped  $ZrO_2$ /zeolite–NaX = 40.80 nm. Therefore the formed  $ZrO_2$  is in a crystallite and nano-form.

FTIR spectroscopy is used to determine the functional groups in zeolite–NaX,  $ZrO_2$  and urea, and it is also used to prove the presence of these materials in the final synthesized nanoparticles. Figure 2a–c shows the FTIR analysis results for the synthesized nanoparticles of zeolite–NaX, synthesized  $ZrO_2$  nanoparticles and pure urea, respectively. Also, in figure 2d, the transmission spectra of N-doped 10 wt%  $ZrO_2$ –zeolite nanoparticles are presented. Figure 2a shows the IR spectrum of the synthesized zeolite–NaX nanoparticles; the highest peak intensity appeared at  $980\text{ cm}^{-1}$  indicates the asymmetric stretching vibration of Si–O–Al in the zeolite framework. The absorption band in the range of  $980$  to  $1320\text{ cm}^{-1}$  shows the presence of substitutional Al atoms in tetragonal forms in the silica structure, which

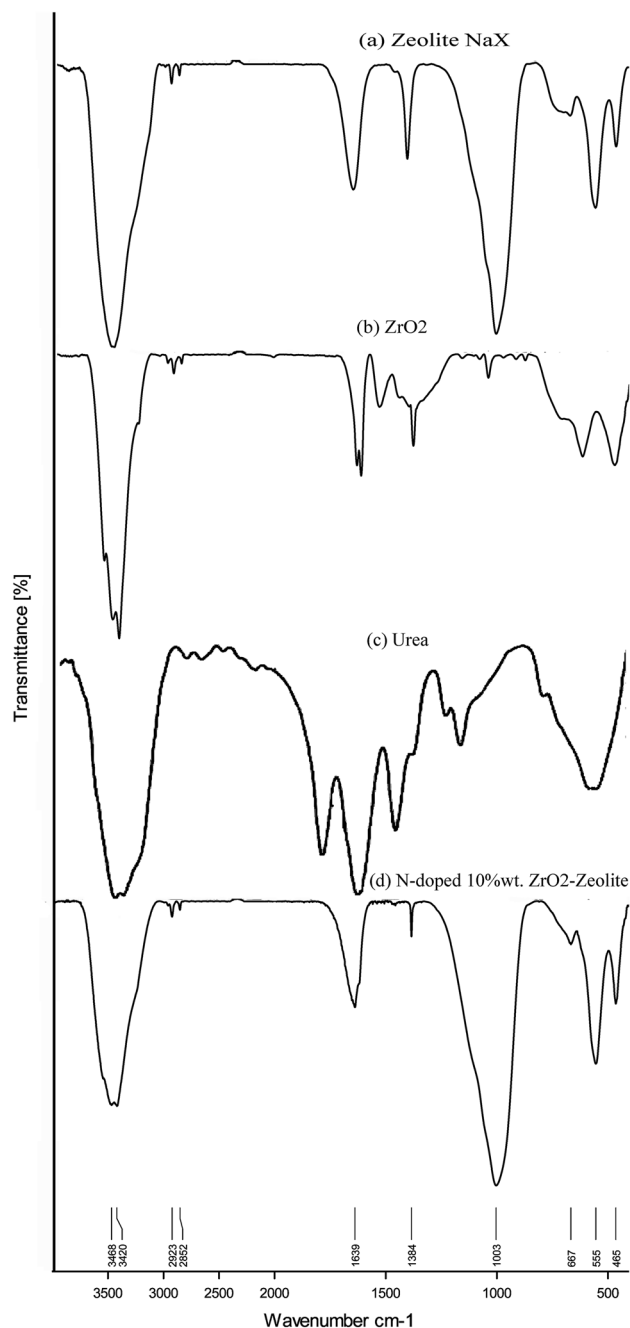


**Figure 2.** FTIR spectra of (a) zeolite–NaX, (b)  $ZrO_2$ , (c) urea and (d) N-doped  $ZrO_2$ –zeolite–NaX.

characterizes the formation of zeolite. Also, the observed absorption band at a wavelength of  $3470\text{ cm}^{-1}$  is related to the stretching vibration of the O–H functional group. The peak obtained at a wavelength of  $1646\text{ cm}^{-1}$  shows the bending state of water molecules. All of these observed specifications confirm the formation of zeolite (Ze–NaX) [14]. In the IR spectrum of the synthesized zirconia nanoparticles (figure 2b), the observed peaks at  $3472$  and  $1639\text{ cm}^{-1}$  are assigned to the structural vibrations of physically adsorbed –OH groups connected with  $Zr^{4+}$  and to scissor bending

mode of coordinated molecular water, respectively [15]. The band at  $1384\text{ cm}^{-1}$  is assigned to the adsorption of non-bridging OH groups. Also, the appeared peak at a wavelength of  $1429\text{ cm}^{-1}$  is corresponding to the absorption of the O–H functional group. The peak observed at a wavelength of  $1049\text{ cm}^{-1}$  can be attributed to one of the zirconyl groups [15].

The absorption bands obtained at  $521$  and  $438\text{ cm}^{-1}$  are related to the monoclinic structure of zirconium ( $m\text{-ZrO}_2$ ), and a sharp peak appeared at a wavelength of  $625\text{ cm}^{-1}$  corresponds to the Zr–O vibrations, associated with the tetragonal structure of  $\text{ZrO}_2$  ( $t\text{-ZrO}_2$ ), which also matches with the XRD results [16]. The urea IR analysis shows a peak at  $1667\text{ cm}^{-1}$  which is attributed to the stretching frequency of C=O bonding. Also, the stretching and deformation frequencies of N–H bonds have been obtained in the wavelength range of  $3455$  and  $1625\text{ cm}^{-1}$ , respectively. The stretching frequency of C–N has appeared at a wavelength of  $1453\text{ cm}^{-1}$  [17]. By comparing figure 2a–c with figure 2d, it is evident that the occurred variations in the peak intensities of  $667$ ,  $1384$ ,  $1639$  and  $3468\text{ cm}^{-1}$  are due to the presence of  $\text{ZrO}_2$  and urea in nanoparticles of N-doped 10 wt%  $\text{ZrO}_2$ -zeolite.

The morphological surface and size of nanoparticles were investigated by SEM. Images obtained from  $\text{ZrO}_2$  nanoparticles and synthesized N-doped  $\text{ZrO}_2$ -Ze are shown in figure 3. As shown in figure 3a, the  $\text{ZrO}_2$  nanoparticles have been adhered together due to the high activity of the surface-to-volume ratio. This phenomenon is also called agglomeration. The aforementioned image confirms the spherical and almost uniform structure with a size of  $\sim 40\text{ nm}$  for nanoparticles. Regarding the obtained SEM image for N-doped  $\text{ZrO}_2$ -Ze photo-catalyst (figure 3b), it can be observed that the  $\text{ZrO}_2$  particles are uniformly distributed at the surface of zeolite; these particles have nanometre dimensions less than  $45\text{ nm}$ . This is due to the successful stabilization of nanoparticles on the zeolite–NaX substrate. From the morphological aspect, the sample contains cubic zeolite and has a relatively uniform size  $< 100\text{ nm}$ .

The textural properties, including the specific surface area, total pore volume and mean pore diameter derived from the  $\text{N}_2$  adsorption–desorption isotherms and pore size distributions of all binary oxides are summarized in table 1.

Table 1 shows that the specific surface area of the 10 wt%  $\text{ZrO}_2$ -zeolite catalyst is less than the pure zeolite–NaX as a result of introducing  $\text{ZrO}_2$ . An increase in the  $\text{ZrO}_2$  content decreases the specific surface area due to an increase in the crystal size and the pore blockage of the support. As compared to 10 wt%  $\text{ZrO}_2$ -zeolite, N-doped 10 wt%  $\text{ZrO}_2$ -zeolite has a higher specific surface area and higher pore volume, but lower average pore diameter. The increased specific surface area after N-doping is probably due to the decreased crystalline size or the formation of more pores with smaller sizes as a result of gas liberation during the decomposition of the zirconium hydroxide–urea complex in the calcination process. It is clearly seen that N-doping has

beneficially altered the textural properties of 10 wt%  $\text{ZrO}_2$ -zeolite.

### 3.2 Photocatalytic process in the presence and absence of light

The dye degradation efficiency vs. time by the dye adsorption of the zirconia nanocatalyst in the absence of UV light, and direct photolysis by UV light without the presence of the catalyst is shown in figure 4. The MO dye sample with a concentration of  $10\text{ mg l}^{-1}$ , the initial pH of solution and a lamp power of  $15\text{ W}$  for  $80\text{ min}$  in the absence of a catalyst was kept under UV light without any additive and oxidation. The results obtained after  $80\text{ min}$  showed that this dye is removed by about 9% without the photocatalyst and under UV light radiation, and that it has a high stability.

The low-decomposition percentage of MO dye in the reference sample is due to the main role of UV light radiation to produce very active hydroxyl radicals. Devi and Rajashekhara [18] and Xin *et al* [19] obtained similar results, dye removal less than 10% by just UV irradiation, in their studies. When the  $\text{ZrO}_2$  photocatalyst was used alone at  $0.1\text{ g l}^{-1}$ , the efficiency of MO dye removing was lower and was found to be about 4%. This shows that the production of hydroxyl radicals, which requires catalysts for the formation, plays a major role in the beginning of dye decomposition. This also proves that the most important factor in initiating and accelerating the photochemical reaction is the simultaneous presence of a catalyst and UV radiation [20], which are discussed below.

### 3.3 Photocatalytic activity of various catalysts

In this work, photocatalytic removal of MO-organic dye by nanophoto-catalysts of  $\text{ZrO}_2$ , zeolite,  $\text{ZrO}_2$ -Ze with different weight percentages and optimized  $\text{ZrO}_2$ -Ze doped with various promoters (nitrogen, copper oxide and cerium oxide) was investigated. This investigation was carried out under operational conditions of initial pH of solution, lamp power of  $15\text{ W}$ , photo-catalyst concentration of  $0.1\text{ g l}^{-1}$  and  $10\text{ mg l}^{-1}$  of MO dye.

### 3.4 Zeolite and pure zirconia catalysts

The MO photocatalytic degradation using catalysts of zeolite and pure  $\text{ZrO}_2$  has been presented in figure 5. The dashed line indicates the beginning of UV irradiation. The results show that the adsorption value for zeolite (about 7%) is more than that for  $\text{ZrO}_2$  (about 4%) in the initial half-hour for the tests which carried out in the dark; this is probably due to the higher surface area of its specific surface. After  $80\text{ min}$  of exposure under UV light, the dye removal percentage for zirconia was achieved by about 37% which is more than that for zeolite (about 30%). The removal rate graph for zeolite, when the equilibrium state was achieved, shows that the MO removal by zeolite was derived from adsorption and photocatalytic processes.

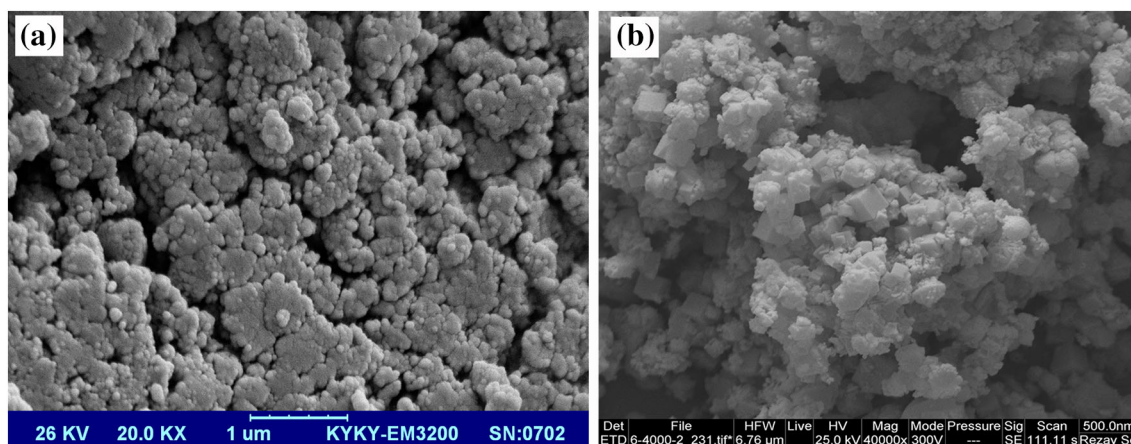


**Figure 3.** SEM images of (a)  $\text{ZrO}_2$  and (b) N-doped  $\text{ZrO}_2$ -zeolite-NaX.

**Table 1.** Textural properties of the prepared materials.

Sample	Surface area ( $\text{m}^2 \text{g}^{-1}$ )	Pore volume ( $\text{cm}^3 \text{g}^{-1}$ )	Average pore diameter (nm)
$\text{ZrO}_2$	76.31	0.09	3.51
Zeolite-NaX	369.5	0.12	1.02
10 wt% $\text{ZrO}_2$ -zeolite	323.5	0.11	2.39
N-doped 10 wt% $\text{ZrO}_2$ -zeolite	356.8	0.12	1.21

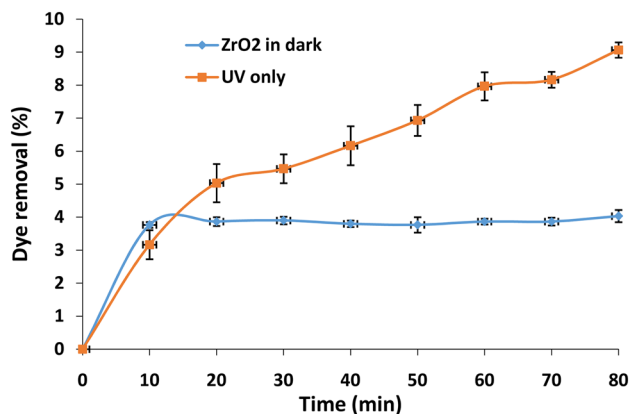


**Figure 4.** Effect of UV light and  $\text{ZrO}_2$  nanoparticles on MO degradation.

As is known, zirconia photocatalytic activity is higher than zeolite which is due to the lower band gap energy of zirconia. The most important limitation for photocatalyst performance is the low adsorption and surface area. Thus, the zirconia stabilization on the adsorbent increases the efficiency and photodecay due to the adsorption of organic molecules and the increase in the organic concentration around the catalyst particles. Stabilization on the surface of an adsorbent facilitates the separation of the catalyst from the dye, reducing its wasting and resulting in better removal of organic pollutants.

Among the various supports that have been investigated for semiconductor stabilization, zeolites are recognized as the best support due to their porous structure, pore size, regular and uniform pores, high adsorption capacity, environmentally friendly and structural photodecay stability (photochemical stability) [5,6].

### 3.5 Combination of zeolite-zirconia catalysts

The MO photo-catalytic decomposition by a combination of  $\text{ZrO}_2$ -zeolite catalysts is presented in figure 5. On comparing the zeolite,  $\text{ZrO}_2$  addition causes an increase in dye removal. By comparing photo-catalytic removal efficiency of four-different ratios of  $\text{ZrO}_2$ -Ze catalysts, the sample with 10 wt% of  $\text{ZrO}_2$  to zeolite had the highest removal rate. The results for 10 wt%  $\text{ZrO}_2$ -zeolite showed that the UV-degradation efficiency has varied from about 30 to 40% relative to pure zeolite in 80 min. The addition of Zr ions provides a large surface charge which acts as an electrical force and increases the efficiency of the separation of the electron-hole pair. Zr ions, also as electronic traps, reduce the surface recombination rate, which maintains the activity of hydroxyl radicals for a long period. In the higher ratios of  $\text{ZrO}_2$ , the mobility of carrier charges decreases, which increases the surface recombination rate and, as a result, shortens the life of hydroxyl radicals [2]. The other reason for lowering the dye removal by increasing the weight percentage of  $\text{ZrO}_2$  can be due to trapping of  $\text{ZrO}_2$

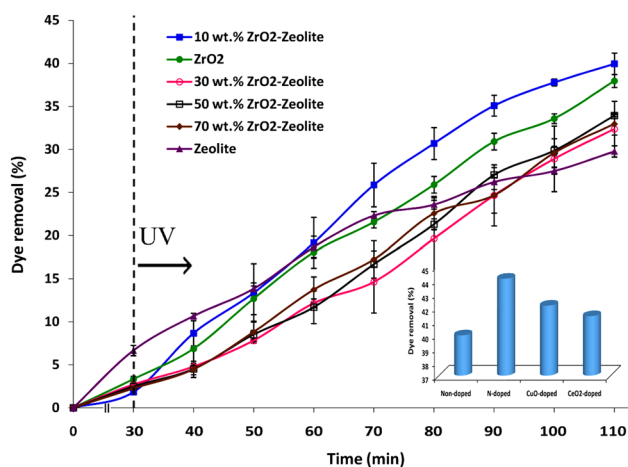


**Figure 5.** MO photocatalytic degradation by different catalysts (scatter chart), effect of doping a 10 wt% ZrO<sub>2</sub>-zeolite nanocatalyst (column chart).

in the pores of the zeolite catalyst, which causes reduction in zeolite adsorption, and ZrO<sub>2</sub> itself is not well deposited at the zeolite surfaces. However, addition of ZrO<sub>2</sub> to zeolite increases the ability of photo-catalytic and adsorption processes. Therefore, adsorbed pollutants on the surface of the catalyst are more affected by produced hydroxyl radicals and increase the decomposition rate of pollutants [8,13].

### 3.6 The doped ZrO<sub>2</sub>-Ze catalyst

In this work, addition of a promoter to increase the photo-catalytic decomposition efficiency was also investigated. The MO photo-catalytic degradation using the optimum catalyst of 10 wt% ZrO<sub>2</sub>-Ze doped by nitrogen, copper oxide and cerium oxide is presented in figure 5 (column chart). As shown in this column chart, the N-doped ZrO<sub>2</sub>-Ze catalyst has the highest dye removal. The photocatalytic degradation of MO by a doped catalyst with nitrogen, copper oxide and cerium oxide after 80 min and exposed under UV light increased by about 44, 42 and 41% shows a better performance when compared with 10 wt% ZrO<sub>2</sub>-Ze catalyst (40%). This increase may be due to several factors. First, the produced electrons during the irradiation of the energy gap may have migrated to nitrogen; resulting in an increase in the reduction rate of oxygen and subsequently, causes to an increase in the oxidation rate [21]. The energy gap is actually the same wavelength that the semiconductor is excited using radiation. Second, in general, metallation and nitration of catalyst surfaces cause an increase in the electron activation, which is the reason for an increase in photo-catalyst activity [2]. Other researchers have suggested that the compounds of the electrostatic layers produce negative-charge particles, which can be considered as an additional level acceptor between the valence and conductivity bands of semiconductors. Therefore, this level adsorbs the positive-holes to the surface of the catalyst and repulses the electrons towards the bulk. This behaviour is similar to

increasing the electron field in photo-catalytic reactions. This behaviour also prevents surface recombination and increases the photo-catalytic degradation rate [22].

### 3.7 Photocatalysis investigation using RSM and statistical analysis

After the determination of the N-doped 10 wt% ZrO<sub>2</sub>-Ze as an optimum photocatalyst, the MO-photocatalytic removal was also investigated using the RSM. The parameters that are considered in the process are the pH, initial concentration of dye, the amount of loaded catalyst and the power consumption of a UV lamp, each of which is considered in three levels. The Box-Behnken design (BBD) was used as one of the experimental design methods to optimize dye removal. The BBD method uses linear regression for empirical results to determine the coefficients of quadratic polynomial equations [23]. Analysis of photocatalytic dye as a function of pH values of 3–9, the initial concentration of dye concentration 5–25 (mg l<sup>-1</sup>), the UV lamp power of 4–15 (W) and the concentration of the catalyst in amounts of 0.1–0.4 (g l<sup>-1</sup>) at the environment temperature was examined. To evaluate the interaction of four-independent parameters on the response function, 27 experiments were designed. The statistical combinations of independent variables with measured values (after 80 min under radiation of UV light) are presented in table 2. Using the obtained results, an empirical relationship between the response and the independent variables, which presented using a quadratic polynomial equation with interactions between independent variables, is obtained. Equation (4) represents the second-order empirical model for dye removing with four dependent variables.

$$\begin{aligned} \text{Dye removal (\%)} = & +24.09 - 3.58A - 15.15B \\ & - 13.07C + 17.53D + 10.06AD \\ & - 11.53BC + 14.38CD + 10.21A^2 \\ & +6.46B^2 + 38.12C^2 - 7.39D^2. \quad (4) \end{aligned}$$

The efficiency of the predicted photo-catalytic conversion is presented using the equation above in the analysis of the variance (ANOVA) table. To interpret the model, tests have been performed to evaluate the efficiency of each model coefficient. The results for the dye removal responses are summarized in the ANOVA table (table 3).

The results show that there is good compatibility between the experimental and predicted values for the photo-catalytic conversion efficiency. The value of the correlation coefficient  $R^2$  is 0.89030, which is acceptable; indicating that the 89.03% of the data variations can be explained by the model. The obtained value of  $F$  is equal to 6.67, which is in agreement with the value of  $F$  presented in the statistical tables, and shows that the gained model is suitable. On the other hand, the value of  $P$  is equal to 0.0654 for the lack of the fit term which indicates that the ratio of the lack of fit to pure error is not significant and the model is acceptable [1]. Also, the value of obtained  $P$  in the analysis of the variance table was

**Table 2.** Box–Behnken experiments along with actual values.

Run	A: catalyst loading (g l <sup>-1</sup> )	B: dye concentration (mg l <sup>-1</sup> )	C: pH	D: UV lamp power (W)	MO removal (%)
1	0.25	5.00	7.00	15.00	35.8
2	0.25	15.00	7.00	8.00	22.7
3	0.40	15.00	9.00	8.00	8.43
4	0.10	15.00	7.00	4.00	21.14
5	0.10	25.00	7.00	8.00	27.27
6	0.25	5.00	3.00	8.00	82.43
7	0.25	15.00	9.00	4.00	3.95
8	0.40	15.00	7.00	15.00	46.84
9	0.25	5.00	7.00	4.00	5.29
10	0.25	25.00	3.00	8.00	79.05
11	0.25	15.00	3.00	15.00	78.2
12	0.25	25.00	7.00	4.00	2.45
13	0.25	15.00	7.00	8.00	19.95
14	0.25	15.00	9.00	15.00	77.1
15	0.40	5.00	7.00	8.00	61.39
16	0.10	15.00	3.00	8.00	91.18
17	0.25	25.00	7.00	15.00	19.66
18	0.40	25.00	7.00	8.00	5.28
19	0.25	25.00	9.00	8.00	4.96
20	0.40	15.00	7.00	4.00	3.8
21	0.25	15.00	3.00	4.00	53.14
22	0.25	5.00	9.00	8.00	39.07
23	0.40	15.00	3.00	8.00	80.63
24	0.10	5.00	7.00	8.00	84.99
25	0.25	15.00	7.00	8.00	13.64
26	0.10	15.00	9.00	8.00	18.45
27	0.10	15.00	7.00	15.00	28.2

**Table 3.** Analysis of variance (ANOVA) for fit of decolourization efficiency from BBD.

Source of variations	Model	Residuals	Lack of fit
Sum of squares	20,409.80	4170.32	4127.17
Degree of freedom	11	15	13
Mean square	1855.44	278.02	317.47
<i>F</i> -value	6.67		14.71
<i>P</i> -value	0.0005		0.0654
<i>R</i> -squared	0.8903		

equal to 0.0005 for the proposed model which is valuable. According to the results of the researchers, the level of significance  $<0.05$  is assumed to be so small that it can be concluded that there is a significant difference between the methods. To summarize, ANOVA for the quadratic model ( $F = 6.67$ ,  $P = 0.0005$ ) shows that the model is acceptable and  $<0.05\%$  probability is due to chance [1,23].

In order to find the maximum area and to investigate the MO removal efficiency, two-dimensional and three-dimensional contour graphs have been used. To study the effect of the amount of the loaded catalyst on the photocatalytic conversion

efficiency, the concentration of MO solution vs. photocatalyst was investigated in the consumption power of UV lamp 15 W and  $\text{pH} = 7$ . As shown in figure 6a, the dye removal percentage is increased with increasing in the amount of the loaded catalyst (N-doped 10 wt% ZrO<sub>2</sub>-zeolite) and decreasing in the concentration of the dye solution. It can also be seen that in the dye concentration range of 5 mg l<sup>-1</sup> and catalyst concentration of 0.1 to 0.4 mg l<sup>-1</sup>, the highest percentage of photo-catalytic removal was obtained which arrived from 59 to 73%. By increasing the photocatalyst concentration, many active sites were produced that cause to increase the removal speed and efficiency. On the other hand, an increase in the photocatalyst concentration causes to increase turbidity and interferes in light passing through the solvent, which cause to reduce the removal rate [1].

Huang and Shu removed the MO dye using a TiO<sub>2</sub>-modified platinum photocatalyst on natural zeolite, and investigated the different concentrations of the catalyst from 1.5 to 6 g l<sup>-1</sup>. The results showed that by increasing the concentration of the catalyst in a range from 5 up to 3 g l<sup>-1</sup>, the amount of decolourization significantly increased from 59.2 to 90.5% from MO solution. Then, this intensity is decreased by increasing the catalyst concentration which is due to the light scattering and screening effect [24]. Several studies have reported



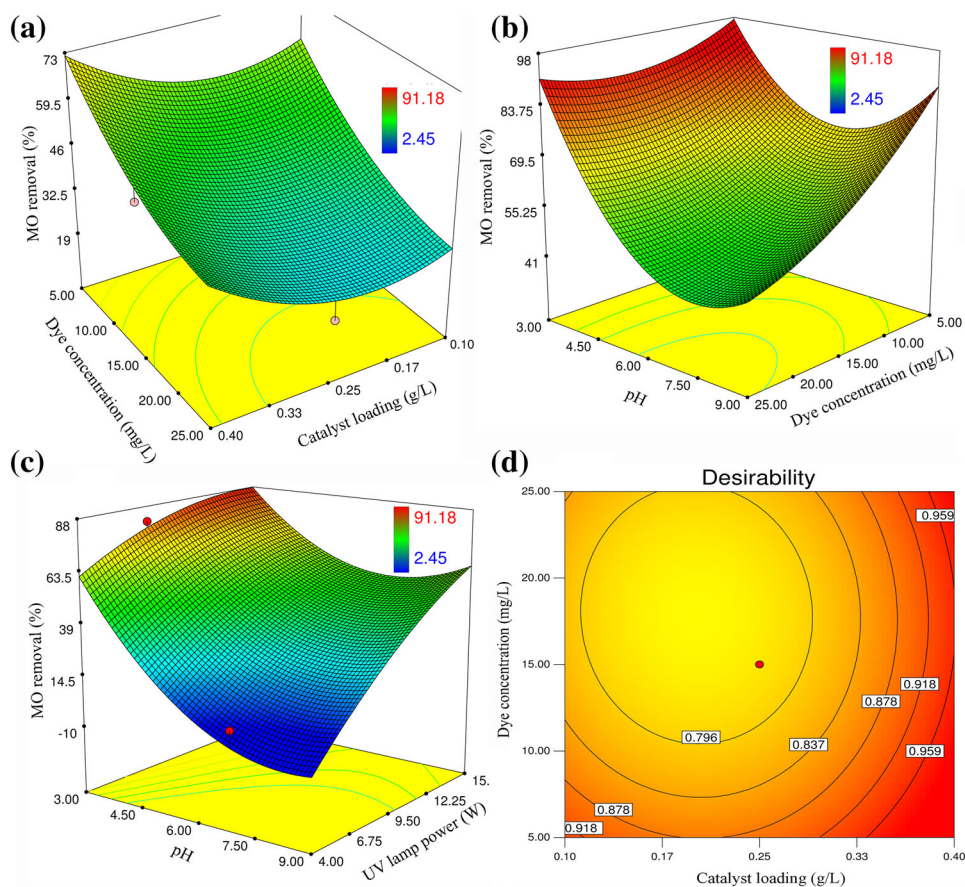


**Figure 6.** Contour plot, (a–c) the effect of operational parameters on MO removal efficiency and (d) the percentage of MO removal under optimal conditions.

that the degradation efficiency is reduced with increasing photocatalyst concentrations over the certain limits [2–5,9–12]. Figure 6b shows the effect of the MO dye concentration and the solution pH on the photocatalytic conversion efficiency at the UV lamp power of 15 W and the catalyst loading of  $0.4 \text{ g l}^{-1}$ . As is clear that the highest percentage of dye removal has been obtained at pH 3 and a dye concentration of  $5 \text{ mg l}^{-1}$ . By increasing the concentration of pollutants, the final removal rate of the dye decreases, which indicates a negative effect of increasing concentration of the reaction. At high dye concentrations, most active sites may be coated with dye ions. This may be a reason to reduce the production of OH radicals on the catalytic surface and will be presented with lower efficiency along with the reduced efficiency of degradation [25]. Barakat in his study stated that the reason for reduction in the percentage of dye at higher concentrations is due to the turbidity and also adsorption on the catalyst surface, followed by the decreasing of active sites [20]. Figure 6c shows three-dimensional contour graph for the photo-catalytic dye removal efficiency as a function of the solution pH and the power consumption of the UV lamp at constant concentration levels of dye solution ( $15 \text{ mg l}^{-1}$ ) and the amount of loaded catalyst ( $0.4 \text{ g l}^{-1}$ ). It is obvious

that the photo-catalytic removal also increases with increasing in the lamp power consumption and decreasing in the pH. The highest dye removal achieves at UV lamp power = 15 W and pH = 3. The higher UV power provides greater energy for the photocatalyst particles to produce the electron–hole pairs, hence, the removal rate increases at higher powers of the UV lamp.

The environmental pH has complex effects on the reaction rate of photocatalytic oxidation. It depends on the adsorption of the pollutant on the catalyst surface, and its degradation rate near the zero point charge of the catalyst. Therefore, the optimum pH of the environment varies depending on the nature of each pollutant [1,21,22]. This index significantly changes the particle surface charge, the oxidation potential and the position of energy bands. Muruganandham *et al* [26] showed that the effect of pH is related to the potential properties of the photocatalytic surface and can be explained based on the potential of zero point (PZC). The pH of PZC for  $\text{ZrO}_2$  and zeolite–NaX is 6.7 and 4.7, respectively. At pH values lower than 6.7 and 4.7, or in other words, in the acidic pH, the catalytic surface receives positive charge, which results in photocatalyst adsorption of anionic and repulsion of cationic compounds. Conversely, at pH values higher than 6.7, the

catalyst surface receives a negative charge, which results in cationic adsorption and anionic compounds being repulsed. Muruganandham *et al* [26] found that by increasing the pH from 1 to 9, the decolourization rate for 14-orange was in the range of 15.16 to 87.28% after 80 min, however, the faster dye removal observes in alkaline pH. In contrast, the study of some azo-dyes showed different results [27]. For example, 17-yellow acid shows the highest degradation at pH 3, and for orange II and Amiddoblack-10B the highest degradation is reported at pH 9 [28]. Zhu *et al* [29], in their study on MO concluded that the highest degree of decolourization that resulted in the removal of 97% of the colour was observed at pH 2, which attributed to the electrostatic absorbance between the positive surface of the catalyst and the MO anion. The reason for the higher process efficiency under acidic pH conditions is that in acidic environments,  $H^+$  ions are absorbed on the surface of  $FeO_2$ . In this case, the generated electrons can increase the number of negative-charge sites using  $H^+$  ions. The number of negative-charge sites on the catalyst surface cannot be effective in the dye removal. Thus, an increase in pH causes a decrease in the photocatalyst ability in the removal of dye. The MO dye is also anionic and hence, in acidic pH, it is better adsorbed on the photocatalyst particle surface with positive charge, and the removal process in acid pH is performed much more effectively than alkaline pH.

In order to select the optimum conditions, in addition to achieving the highest removal percentage in the highest pollutant concentration, lower consumption of the catalyst is considered to reduce the costs. Two-dimensional contour graph in figure 6d shows the performance removal contour for MO-dye and gained optimal level based on the loaded catalyst ( $g\ l^{-1}$ ), initial concentration of dye ( $mg\ l^{-1}$ ), UV lamp consumption power of 15 W and pH = 3. As can be seen, one of the optimal points with the highest catalytic decomposition can be determined at an initial concentration of 5 ppm, pH 3, loading catalyst of  $0.4\ g\ l^{-1}$  and the lamp power of 15 W.

### 3.8 Kinetic study of photocatalytic removal reaction

The reaction kinetics for heterogeneous catalytic systems are described by kinetic models in which reactions begin with adsorption of matter on the solid phase. In this model, the adsorption on the catalyst is assumed to be an elementary reaction [30].

One of these models is the Langmuir–Hinshelwood model, in which the material is absorbed on the catalyst and then the chemical reaction takes place at the catalyst surface. The model is as follows:

$$-\frac{dC}{dt} = \frac{k_r K_e C}{1 + K_e C}, \quad (5)$$

where  $k_r$  and  $K_e$  are the kinetic constant of the Langmuir–Hinshelwood and the Langmuir kinetic constant, respectively.

With assuming first-order kinetics for the case with low concentration of pollutants, the above relationship will represent the kinetic of the first-order reaction. Integrating equation (5), with initial condition of  $C = C_0$  at  $t = 0$ , gives:

$$\ln\left(\frac{C}{C_0}\right) = -k_{app}t, \quad (6)$$

where  $k_{app}$  is a superficial speed of the first-order reaction. The above pseudo first-order kinetic has been reported in many photocatalytic studies [30–32]. The rate constant was estimated from the slope of  $\ln(C/C_0)$  vs. time, plotted under optimized conditions. The obtained  $k_{app} = 0.031\ min^{-1}$  from this investigation shows the high-constant speed of the reaction under the optimized conditions, which is also proving the efficiency of the used optimization methods of the reaction.

## 4. Conclusions

In this study, the efficiency of loaded  $ZrO_2$  nanoparticles on the zeolite–NaX as a photocatalyst exposed under UV radiation for degradation of MO-dye from water was investigated. Complete removal of MO was achieved using N-doped 10 wt%  $ZrO_2$ –zeolite. The effect of the initial concentration of the contaminants on the photo-catalytic degradation showed that by increasing the initial concentration of MO from 5 to  $25\ mg\ l^{-1}$ , the photo-catalytic degradation rate decreases. This is due to the high absorption of UV light at very high concentrations, and as a result, the solution acts as an effective internal filter. Under these conditions, a smaller portion of the photons reaches to the semiconductor, and subsequently the production efficiency of hydroxyl radicals and the rate of degradation decreases. It was also found that increasing the concentration of the loaded nanocatalyst in the dye solution increases the amount of dye degradation. According to the results, it was found that the percentage of dye degradation with the power consumption of the UV lamp had a linear relation. Increasing the power of the UV lamp increases the energy of nanoparticles in order to produce an electron–hole pair, thus the removal rate raised at higher power of UV lamps. The results also showed that the pH plays an important role in the removal rate of MO contamination, so that the photocatalytic degradation of this anionic pollutant in acidic pH has a much higher efficiency than in a neutral and alkaline pHs. The physical properties of the synthesized nanoparticles were also determined using XRD, FTIR, SEM and BET. The SEM image showed that  $ZrO_2$  nanoparticles have a spherical structure and uniform with size distribution approximately equal to 40 nm, and that  $ZrO_2$  particles are uniformly dispersed on a cubic surface of zeolite. In general, the results of this study showed that the nanophotocatalyst of N-doped 10 wt%  $ZrO_2$ –zeolite has a high efficiency for the degradation of anionic MO-dyes and can be used as an efficient option

for purifying coloured dye and destroying environmental pollutants.

### Acknowledgements

MM thanks the University of Ilam, for the award research fellowship.

### References

- [1] Mansouri M, Tanzifi M, Lotfi H and Nademi M 2017 *St. Cerc. St. CICBIA* **18** 153
- [2] Alalm M G, Ookawara S, Fukushi D, Sato A and Tawfi A 2016 *J. Hazard. Mater.* **302** 225
- [3] Ahmad T, Shahazad M and Phul R 2017 *Mater. Sci. Eng. Int. J.* **1** 100
- [4] Mahadwad O K, Parikh P A, Jasra R V and Patil C 2011 *Bull. Mater. Sci.* **34** 551
- [5] Khatamian M, Hashemian S and Sabaee S 2010 *Mater. Sci. Semicond. Process.* **13** 156
- [6] Ökte A N and Yilmaz Ö 2008 *Appl. Catal. B* **85** 92
- [7] Bhattacharjee S, Sarkar S H, Raybarman U and Panja J 2016 *Int. J. Innov. Res. Sci. Technol.* **2** 284
- [8] Panpa W, Sujaridworakun P and Jinawath S 2008 *Appl. Catal. B* **80** 271
- [9] Zhao J, Wang X, Zhang L, Hou X, Li Y and Tang C 2011 *J. Hazard. Mater.* **188** 231
- [10] Ismail S, Ahmad Z A, Berenov A and Lockman Z 2011 *Corros. Sci.* **53** 1156
- [11] Basahel S N, Ali T T, Mokhtar M and Narasimharao K 2015 *Nanoscale Res. Lett.* **10** 73
- [12] Yoa S, Jia X, Jiao L, Zhu C and Shi Z 2012 *Indian J. Chem.* **51A** 1049
- [13] Mzoughi M, Anku W W, Oppong S O B, Shukla S K, Agorku E S and Govender P P 2016 *Res. Artic. Adv. Mater. Lett.* **7** 946
- [14] Amaladhas P T and Thavamani S S 2013 *Adv. Mater. Lett.* **4** 688
- [15] Ivanova T, Harizanova A, Koutzarova T and Vertruyen B 2010 *Cryst. Res. Technol.* **45** 1154
- [16] Hao Y, Li J, Yang X, Wang X and Lu L 2004 *Mater. Sci. Eng. A* **367** 243
- [17] Manivannan M and Rajendran S 2011 *Int. J. Eng. Sci. Technol.* **3** 8048
- [18] Devi L G and Rajashekhar K E 2011 *J. Mol. Catal. A: Chem.* **334** 65
- [19] Xin W, Zhu D, Liu G, Hua Y and Zhou W 2012 *Int. J. Photoenergy* **2012** 1
- [20] Barakat M 2011 *J. Hydro. Environ. Res.* **5** 137
- [21] Zhao S, Ramakrishnan G, Shen P, Su D and Orlov A 2013 *Chem. Eng. J.* **217** 266
- [22] Chakrabarti S and Dutta B K 2004 *J. Hazard. Mater.* **112** 269
- [23] Mansouri M, Atashi H, Khalilipour M M, Setaresheenas N and Shahraki F 2013 *J. Korean Chem. Soc.* **57** 769
- [24] Huang C R and Shu H Y 1995 *J. Hazard. Mater.* **41** 47
- [25] Espino-Estévez M R, Fernández-Rodríguez C, González-Díaz O M, Araña J, Espinós J P, Ortega-Méndez J A *et al* 2016 *Chem. Eng. J.* **298** 82
- [26] Muruganandham M, Shobana N and Swaminathan M 2006 *J. Mol. Catal. A: Chem.* **246** 154
- [27] Sakthivel S, Neppolian B, Murugesan L and Venkatakri S H 2003 *Sol. Energy Mater. Sol. Cells.* **77** 65
- [28] Qamar M, Saquib M and Muneer M 2005 *Dyes Pigm.* **65** 1
- [29] Zhu H, Jiang R, Fu Y, Guan Y, Xiaob L, Yao J *et al* 2012 *Desalination* **286** 41
- [30] Nodehi A, Atashi H and Mansouri M 2019 *J. Dispersion Sci. Technol.* **40** 766
- [31] Arabi A, Fazli M and Ehsani M H 2018 *Bull. Mater. Sci.* **41** 77
- [32] Ahmed T, Phul R, Alam P, Lone I H, Shahazad M, Ahmed J *et al* 2017 *RSC Adv.* **7** 27549